.

Ag films grown by remote plasma enhanced atomic layer deposition on different substrates

Akinwumi A. Amusan and Bodo KalkofenHassan Gargouri, Klaus Wandel, and Cay PinnowMarco LiskerEdmund P. Burte

Citation: J. Vac. Sci. Technol. A **34**, 01A126 (2016); doi: 10.1116/1.4936221

View online: http://dx.doi.org/10.1116/1.4936221

View Table of Contents: http://avs.scitation.org/toc/jva/34/1

Published by the American Vacuum Society

RIGHTSLINK
Copyright Clearance Center

Ag films grown by remote plasma enhanced atomic layer deposition on different substrates

Akinwumi A. Amusan[a)] and Bodo Kalkofen
Institute of Micro and Sensor Systems, Otto-von-Guericke University, Universitätsplatz 2, 39106 Magdeburg, Germany

Hassan Gargouri, Klaus Wandel, and Cay Pinnow
SENTECH Instruments GmbH, Schwarzschildstraße 2, 12489 Berlin, Germany

Marco Lisker
IHP, Im Technologiepark 25, 15236 Frankfurt (Oder), Germany

Edmund P. Burte
Institute of Micro and Sensor Systems, Otto-von-Guericke University, Universitätsplatz 2, 39106 Magdeburg, Germany

(Received 7 August 2015; accepted 10 November 2015; published 23 November 2015)

Silver (Ag) layers were deposited by remote plasma enhanced atomic layer deposition (PALD) using Ag(fod)(PEt_3) (fod = 2,2-dimethyl-6,6,7,7,8,8,8-heptafluorooctane-3,5-dionato) as precursor and hydrogen plasma on silicon substrate covered with thin films of SiO_2, TiN, Ti/TiN, Co, Ni, and W at different deposition temperatures from 70 to 200 °C. The deposited silver films were analyzed by x-ray photoelectron spectroscopy (XPS), atomic force microscopy (AFM), scanning electron microscopy (SEM), transmission electron microscopy (TEM) with energy dispersive x-ray spectroscopy, four point probe measurement, ellipsometric measurement, x-ray fluorescence (XRF), and x-ray diffraction (XRD). XPS revealed pure Ag with carbon and oxygen contamination close to the detection limit after 30 s argon sputtering for depositions made at 120 and 200 °C substrate temperatures. However, an oxygen contamination was detected in the Ag film deposited at 70 °C after 12 s argon sputtering. A resistivity of 5.7×10^{-6} Ω cm was obtained for approximately 97 nm Ag film on SiO_2/Si substrate. The thickness was determined from the SEM cross section on the SiO_2/Si substrate and also compared with XRF measurements. Polycrystalline cubic Ag reflections were identified from XRD for PALD Ag films deposited at 120 and 200 °C. Compared to W surface, where poor adhesion of the films was found, Co, Ni, TiN, Ti/TiN and SiO_2 surfaces had better adhesion for silver films as revealed by SEM, TEM, and AFM images. © *2015 American Vacuum Society*. [http://dx.doi.org/10.1116/1.4936221]

I. INTRODUCTION

One of the difficult challenges for future interconnects as identified by the International Technology Roadmap for Semiconductor (ITRS—Interconnect) in the near term (greater than 16 nm maximum half pitch) is the introduction of new materials that meet the wire conductivity requirements and reduced dielectric permittivity.[1] Silver has the lowest resistivity ($\approx 1.6 \times 10^{-6}$ Ω cm) of all metals and a low residual stress compared to copper,[2] and down scaling to sub-100 nm is possible without a substantial increase in resistivity. Silver is therefore considered as a potential replacement for copper in interconnects and contacts. However, one drawback of silver metallization might be reliability. Silver diffuses at high temperature and also corrodes at higher bias voltage. A threshold voltage of 3 V was observed for accelerated silver corrosion in structures with 100 μm line width.[2] However, silver is still useful for future interconnects because the operating voltage is also scaling down. In addition, silver metallization requires suitable adhesion promoter to allow growth of continuous silver layer as well as barrier layer to prevent diffusion of silver into silicon. Plasma assisted atomic layer deposition (PALD) technique for silver deposition has potential benefits such as an excellent surface and step coverage, a precise control of deposition, and is also compatible with silicon microfabrication. As a proposed application, the PALD silver layers can be used as seed layers for silver electroplating, especially in high aspect ratio structures required for multilevel interconnects. Besides microelectronics application, silver coating is also useful in plasmonics,[3] highly reflective mirrors,[4] antimicrobial coating,[5] gas sensors,[6] catalyst,[7] and decorations. Some work on plasma enhanced layer deposition of silver have been reported[8–10] with Ag(fod)(PEt_3) (fod = 2,2-dimethyl-6,6,7,7,8,8,8-heptafluorooctane-3,5-dionato) suggested to be the best choice of precursor so far.[8] Very recently, Bruele *et al.*[10] demonstrated the spatial plasma enhanced atomic layer deposition of silver at atmospheric pressure, where it was shown that the film morphology is highly dependent on Ag surface diffusion controlled by the deposition temperature, and they concluded that high Ag growth rate at lower deposition temperature will favor growth of thin continuous silver layers. Here, in this work, we aim to investigate the deposition of silver layers by PALD using Ag(fod)(PEt_3) as a precursor and hydrogen radicals generated by a remote low pressure (0.01–1 mbar)

[a)]Electronic mail: akinwumi.amusan@ovgu.de

RIGHTSLINK

inductively coupled plasma,[11] on different substrates such as trenches of silicon covered with Ti/TiN (titanium/titanium nitride) layers as well as on planar silicon surface covered with thin layers of SiO_2 (silicon oxide), TiN, Co (cobalt), Ni (nickel), and W (tungsten). We also aim to find suitable adhesion promoter/barrier layers for the growth of continuous Ag films by plasma assisted atomic layer deposition.

II. EXPERIMENT

A. PALD reactor description

The depositions were carried out in a PALD reactor developed by Sentech Instruments GmbH (Fig. 1). It is a single wafer PALD reactor with two heated precursor lines, with one line capable of dosing precursor using the bubbler configuration (line 1). The silver precursor was dosed from a vertical electropolished stainless steel bubbler controlled by fast acting valves with argon used as carrier gas. The reactor walls and precursor lines were heated to 120 °C to avoid precursor condensation while the wafer was heated by the susceptor plate carrying it. Hydrogen plasma radicals were generated in a remote microwave inductively coupled plasma (ICP). The ICP source is a prototype still under development and is made up of a copper resonator (screened within aluminum housing) that excites plasma simultaneously in two quartz discharge tubes of 5 mm internal diameter.[11] Both discharge tubes are powered by a common GaAs microwave power generator at about 2.45 GHz with a maximum output power up to 50 W. A low frequency ignition pulse (500–700 ms) of about 6 kV is applied to create seed plasma that is then sustained by the inductively coupled microwave power. This source is mounted as compact module on the top plate of the PALD reactor. The electric field is predominantly parallel to the capillary walls in the ICP source, and thus, there is negligible etching of the capillary walls that could lead to film contamination. In addition, the plasma parameters such as plasma power and frequency can be controlled independently of substrate parameters in the ICP source. Atomic O, N, and H radicals can be generated with flux densities greater than $2 \times 10^{16}\,cm^{-2}s^{-1}$ using gas flows of 100–300 sccm.

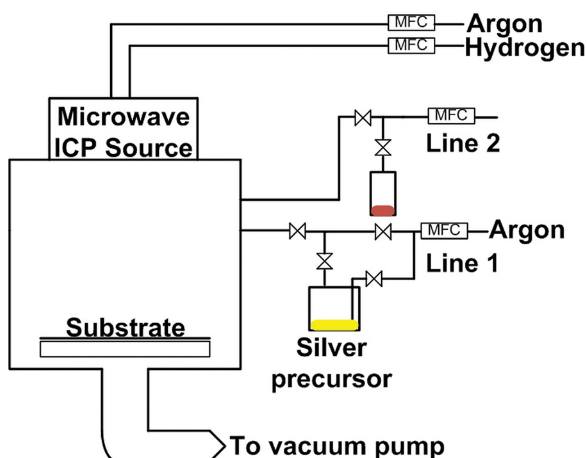

FIG. 1. (Color online) Basic description of the PALD reactor.

B. Process parameters

Depositions were carried out on prepared coupons (about $10 \times 10\,mm^2$) of Si trenches covered with Ti/TiN thin film and planar Si covered with thin films of SiO_2, TiN, Co, Ni, and W. SiO_2 was prepared by thermal oxidation of Si in a furnace. Ti, TiN, Co, and Ni thin films were deposited by physical vapor deposition (sputter deposition). W films were deposited by chemical vapor deposition followed by chemical mechanical polishing to obtain a starting rms roughness of 2 nm. The samples were always placed around the center of the susceptor just beneath the outlet of the discharge tubes in all experiments for an efficient plasma radical supply. The precursor lines and chamber walls were kept at 120 °C temperature while depositions were carried out at 70, 120, and 200 °C substrate temperatures. The silver precursor used was Ag(fod)(PEt_3) (fod = 2,2-dimethyl-6,6,7,7,8,8,8-heptafluorooctane-3,5-dionato), which has a very low vapor pressure and suggested to be thermally stable up to 230 °C by the thermogravimetric measurement.[8] Therefore, the precursor bubbler was maintained at 110 °C temperature. Precursor dosing was done using bubbling configuration, where controlled fast acting valves switch the carrier gas through the precursor bottle during precursor pulse times. As shown in the process sequence (Fig. 2), 50 sccm argon was used as a carrier and purge gas. A mixture of 50 sccm argon and 200 sccm hydrogen was also used for an efficient hydrogen plasma discharge. Hydrogen gas was switched off during silver pulse time to avoid possible CVD reaction at higher temperature while argon flow of 250 sccm was maintained through the plasma source in order to block Ag precursor back flow into the plasma source. Typical process times (pulse/purge) were 2/2 s for silver precursor and 10/1 s for hydrogen plasma at 50 W plasma power. Some plasma pretreatments (about 3 min) were also used for removing native oxides of the metallic surfaces before starting the silver deposition.

C. Film characterization

The optical properties of the silver layer were measured by spectroscopic ellipsometry with SE 850 from Sentech Instruments GmbH using wavelength range from 280 to 850 nm. It was possible to measure the transparent silver layers with reasonable ellipsometric fit using the Brendel

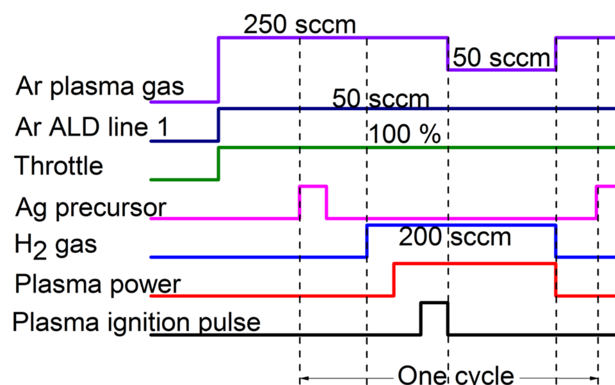

FIG. 2. (Color online) Illustration of PALD process sequence.

RIGHTSLINK

oscillator layer model. Thicknesses of nontransparent silver layers were measured by combining both scanning electron microscope (SEM) cross section and x-ray fluorescence (XRF) measurements (Fischerscope X-ray XDV-SDD from Fischer Technology). The elemental compositions of the film were determined by XPS in an ESCA 5600 of Perkin Elmer. The film morphologies were measured by AFM (Veeco Dimension 3100 in tapping mode), SEM, and TEM. The statistics of Ag particles were analyzed with the commercial SPIP imaging software from Image Metrology A/S and the Origin software. The film crystal structures were determined by x-ray diffraction (XRD) with a Bruker/AXS D5000 diffractometer. The Ag electrical resistivities were determined from the sheet resistances measured with an ordinary four point probe (CDE ResMap 168).

III. RESULTS AND DISCUSSION

A. Film deposition and properties

The silver layers were successfully deposited on all the substrates (SiO_2, TiN, Ti/TiN, Co, Ni, and W surfaces) at 70, 120, and 200 °C deposition temperatures. A maximum growth per cycle of approximately 0.03 nm was obtained from Ag film thickness of more than 500 PALD cycles at all the three deposition temperatures. The samples of Ag layers on TiN surface were analyzed by XPS in order to eliminate the effect of oxygen contamination from an oxide surface. Pure Ag was obtained from the XPS measurement with carbon and oxygen contamination close to the detection limit (Fig. 3) after 30 s argon sputtering for deposition performed at 120 and 200 °C temperatures, which indicate the complete removal of ligand by the hydrogen plasma. A large oxygen contamination was detected in the film for deposition carried out at 70 °C, which means there could be incomplete ligand removal or possible precursor condensation at this low temperature. For all the Ag PALD samples, oxygen and carbon were detected in the as deposited state due to adsorption of organic molecules on the surface. XPS analysis of PVD Ag layers grown by electron beam evaporation for comparison also had carbon and oxygen contamination on the surface, which reduced to detection limit after argon sputtering. The film morphology of silver films of different PALD cycles was also studied using AFM. The Ag particle size distributions from the AFM images for 500 PALD cycles and 1500 PALD cycles were analyzed with SPIP image analysis software. The distributions were fitted into lognormal function as supposed in literature[10] using the ORIGIN software. The diameter of silver particles (Fig. 4) increases with the number of PALD cycles, which shows that the Ag film grows in Volmer Weber mode on all the substrates, where the growth starts from appearing of isolated silver islands to percolation and then bulk regime. The particle size distributions on SiO_2 and TiN surface were identical, which means that growth and coalescence of Ag islands could be identical on both surfaces. The average particle sizes and distributions on the metal surfaces (Co, Ni, and W) were slightly larger at 1500 cycles, which indicates that wetting and coalescence of Ag islands might indeed be faster on metal surfaces. In addition,

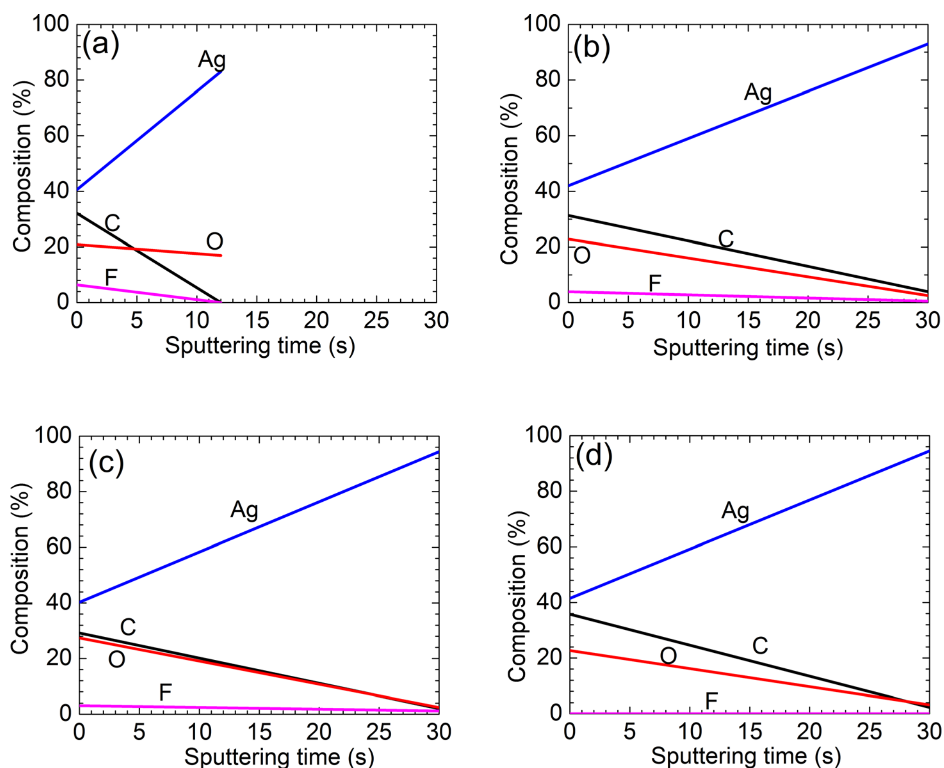

Fig. 3. (Color online) Chemical composition by XPS of PALD Ag films [(a), (b), and (c)] at different deposition temperatures compared with PVD Ag film (d): (a) 70 °C deposition temperature, (b) 120 °C deposition temperature, (c) 200 °C deposition temperature, and (d) PVD Ag film.

RIGHTSLINK

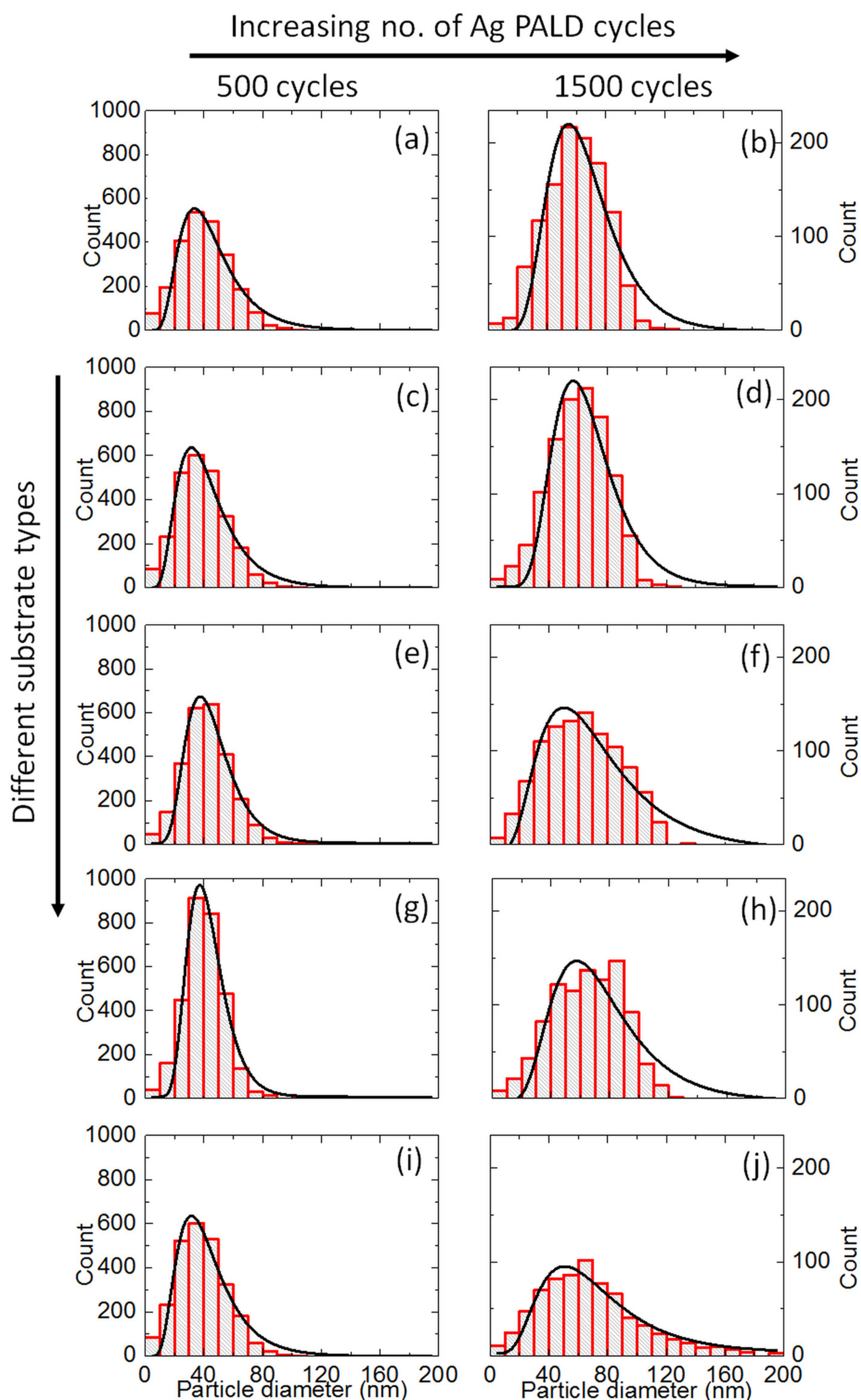

FIG. 4. (Color online) Distribution of particle sizes for PALD Ag films grown at 120 °C deposition temperature on different substrates: (a) and (b)—TiN substrate, (c) and (d)—SiO_2 substrate, (e) and (f)—Co substrate, (g) and (h)—Ni substrate, (i) and (j)—W substrate, (a), (c), (e), (g), and (i)—500 PALD cycles, and (b), (d), (f), (h), and (j)—1500 PALD cycles. Black line curves are lognormal fit.

the rms roughness Rq (Fig. 5) increased as the Ag film gets thicker, with silver on cobalt surface having the lowest roughness followed by titanium nitride, silicon oxide, and nickel surfaces at 3068 Ag PALD cycles. Silver grew on tungsten surface with the highest surface roughness (Rq) as revealed by AFM images (Fig. 6).

The XRD measurements of the PALD silver layers (Fig. 7) grown at 120 and 200 °C deposition temperatures as well as of the PVD silver layers both reveal polycrystalline cubic silver. Silver PALD grown at 70 °C deposition temperature also shows the appearance of Ag[111] peak in the spectra for a much lower film thickness.

RIGHTSLINK

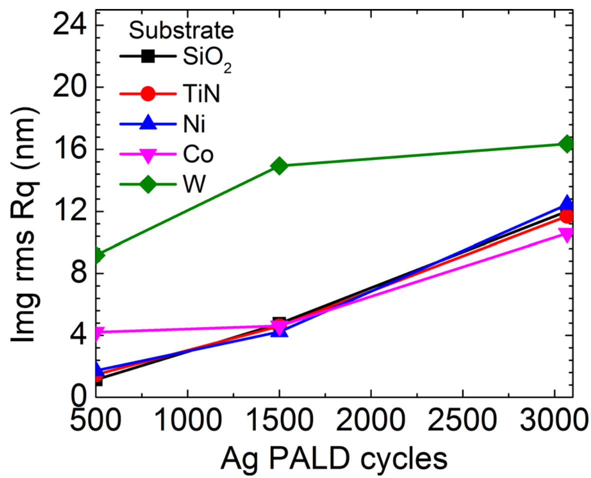

FIG. 5. (Color online) Surface roughness of PALD Ag films grown on different substrates at 120 °C deposition temperature for varying PALD cycles.

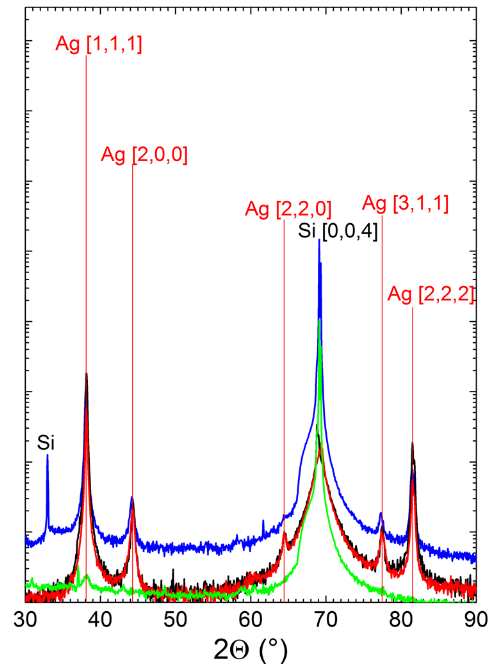

FIG. 7. (Color online) Crystallinity of PALD Ag films compared with PVD Ag.

B. Adhesion of PALD silver layers on different substrates

Wetting of liquids on solid substrate is determined by the equilibrium spreading parameter, which depends on the surface energies of the system. Suppose a liquid spreads on a solid substrate, the equilibrium spreading parameter S_{eq} is defined as[12]

$$S_{eq} = \gamma_{sub} - \gamma_l - \gamma_{int}, \tag{1}$$

where γ_{sub} is the surface energy of the substrate, γ_l is the surface energy of the liquid, and γ_{int} is the surface energy of the interfacial layer between the substrate and the liquid. If $S_{eq} \geq 0$, then the liquid completely wets the substrate, but if $S_{eq} < 0$, then the liquid partially wets the substrate. The same analogy can be used for wetting of metal film on oxide substrate where it was suggested that a metal film will only completely wet an oxide surface in the case when[13]

$$\text{At equilibrium, } \gamma_{metal-oxide} = \gamma_{oxide-v} - \gamma_{metal-v}, \tag{2}$$

where $\gamma_{metal-oxide}$ is the surface energy of the interfacial film between the oxide and the metal, $\gamma_{oxide-v}$ is the pure surface energy of the oxide substrate in vacuum, and $\gamma_{metal-v}$ is the pure surface energy of the metal film in vacuum. Since oxides generally have a lower vacuum surface energy than metals, wetting of metal film on oxide substrate may only be possible when the metal surface energy is lowered by minimizing its own surface area during growth,[14] which explains why the growth of metal on oxide surface is usually from the appearance of metal islands before continuous growth. It is obvious from Eq. (2) that replacing the oxide substrate with a higher surface energy substrate than the deposited metal should, in principle, allow continuous growth of thin metal film on higher surface energy substrate. Tungsten (surface energy of 3.5 J m^{-2}) was used as a substrate to grow ultrathin platinum (surface energy of 2.5 J m^{-2}) layers by atomic layer deposition, and the method was suggested to be more general for growing other lower surface energy metals.[14,15]

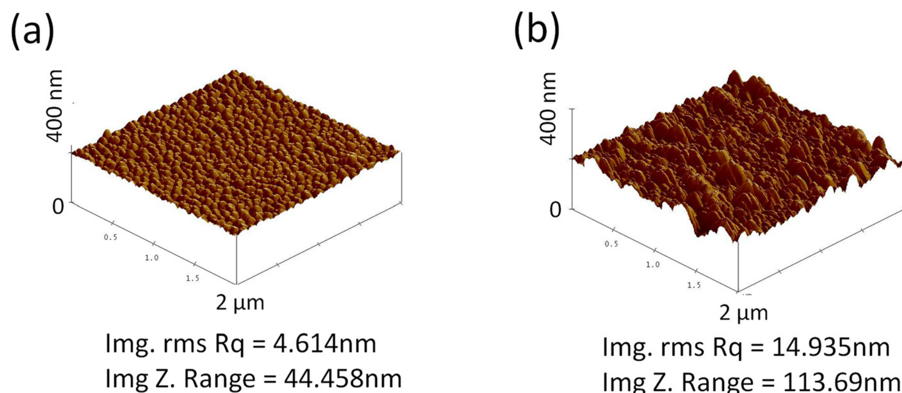

FIG. 6. (Color online) Morphology of PALD Ag films grown on cobalt surface compared with PALD Ag films grown on tungsten surface: (a) Ag on Co surface and (b) Ag on W surface; process—1500 cycles at 120 °C deposition temperature.

RIGHTSLINK

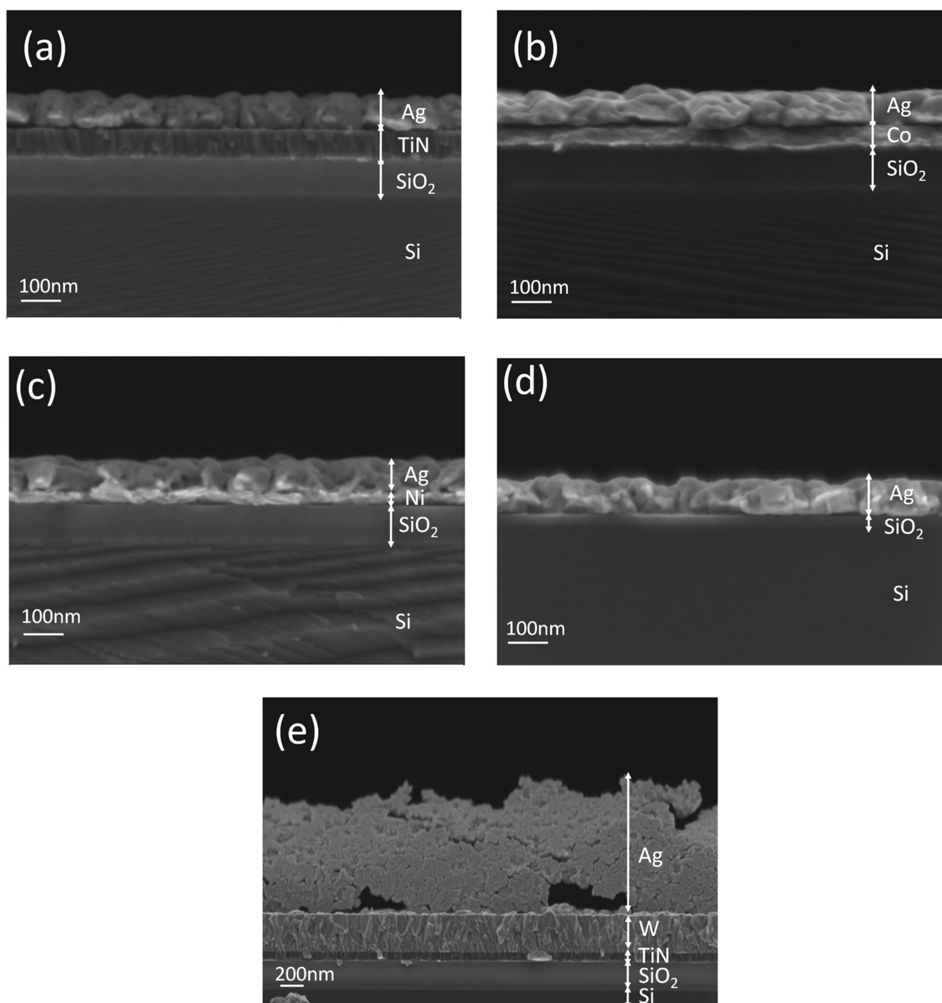

FIG. 8. Comparison of SEM cross sectional image of PALD Ag films grown on different substrates: (a) Ag on TiN surface, (b) Ag on Co surface, (c) Ag on Ni surface, (d) Ag on SiO_2 surface, and (e) Ag on W surface; process—3068 cycles at 120 °C deposition temperature.

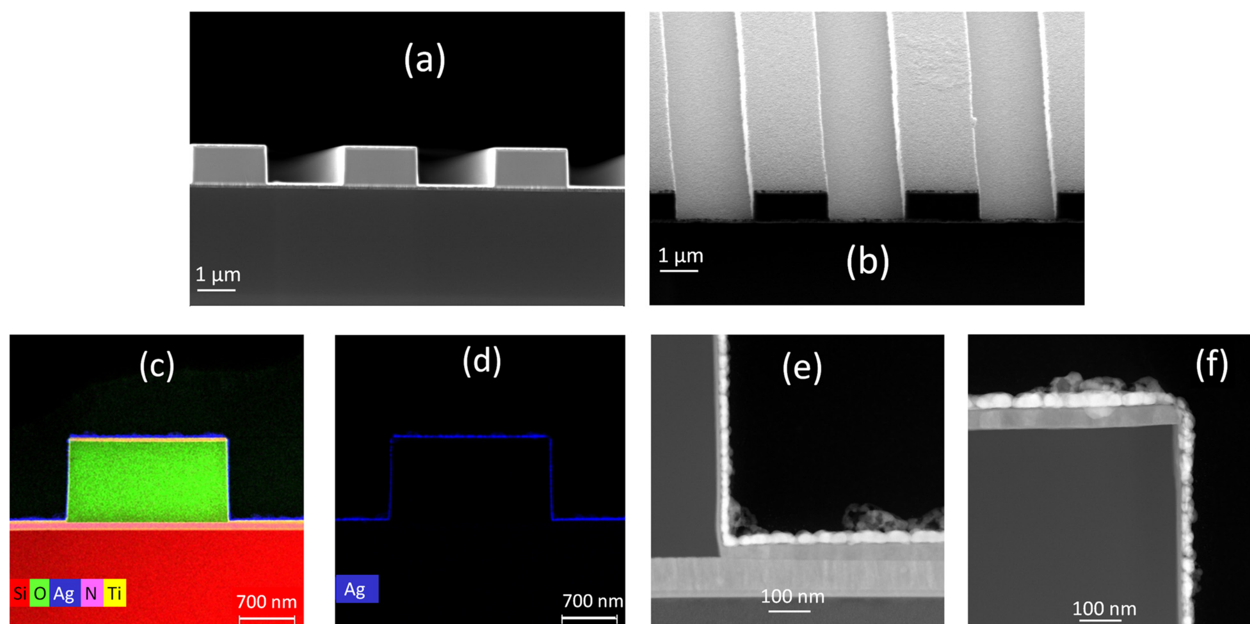

FIG. 9. (Color online) SEM and TEM cross sectional image of PALD Ag film deposited at 120 °C on Ti/TiN/SiO_2/Si trenches of 2 μm width and 1 μm depth: (a) SEM trench cross section; (b) SEM top view; (c) TEM cross section showing film composition with EDX; (d) TEM cross section showing Ag; (e) bottom and side walls (TEM); and (f) top and side walls (TEM).

RIGHTSLINK

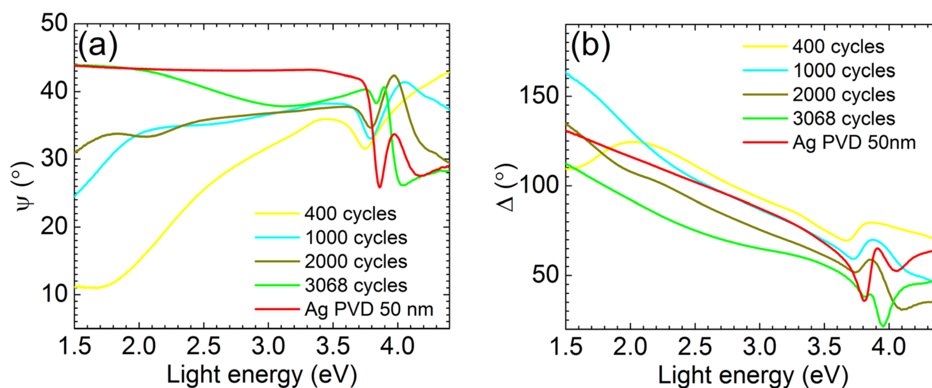

FIG. 10. (Color online) Ellipsometric spectra of Ag films on SiO_2/Si substrate: (a) ellipsometric angle ψ and (b) ellipsometric angle Δ.

Ag, Co, Ti, and Ni have experimental surface energies of 1.25, 2.55, 2.1, and 2.45 J m^{-2}, respectively.[16] It would be expected theoretically that Ag should completely wet Co, Ni, Ti, and W surfaces and coalescence of Ag should be faster on higher surface energy substrates than itself. In addition, oxide and nitride surfaces would have much lower surface energy than metals and the growth mode would start from the Volmer Weber mode before layer by layer growth. The plasma assisted atomic layer deposition of Ag on Co, Ni, W, Ti/TiN, TiN, and SiO_2 surfaces were experimentally demonstrated (Figs. 8 and 9), showing that silver had good adhesion during PALD growth on Co, Ni, TiN, Ti/TiN, and SiO_2 but not on W surface. Among the high surface metal studied, Ag had a better wetting and grew smoothly on Co, Ni, and Ti surface than on W surface. In addition, the Ag films appear more compact as expected on Co and Ni than on SiO_2 and TiN surface. After several cycles, Ag also grew smoothly on TiN and SiO_2 surface as seen in the SEM images. However, the SEM images (Fig. 8) also showed that the silver layers might be flaking off during or after PALD growth on W surface. As a result, the Ag layer on W surface is less compact, rougher, and contains voids in the film and near the substrate. One possible reason to explain this is that the surface of tungsten would have formed a native oxide in air with much lower surface energy (approximately 0.35–1.62 J m^{-2} by simulation).[17] The metallic surfaces were not grown *in situ* with PALD silver and could have possibly formed native oxide in air. Samples were always pretreated with hydrogen plasma for about 3 min duration at 50 W power before starting the Ag PALD; however, it could be that the native oxide of tungsten cannot be completely removed by this hydrogen plasma pretreatment, as also suggested in Ref. 15. The use of wet chemical etching before plasma dry etching could help to remove most of the native tungsten oxide; however, this was not used in this work.

The results of Ag PALD on trenches of silicon via of 2 μm width and 1 μm depth (aspect ratio of 0.5) covered with thin Ti/TiN layers are shown in Fig. 9. The silver deposition gave an estimated step coverage of about 0.6 on these trench structures for about 40 nm Ag film thickness as measured with the SPIP imaging software. It can be observed that the Ti seed layers also had about 0.5 step coverage, which might have made the growth of Ag layers to be slightly retarded on the side walls compared to the top and bottom of the trenches. Carbon and oxygen can also be seen on the surface of the film but not in the bulk silver as measured with energy dispersive x-ray spectroscopy (EDX) and also in agreement with the earlier XPS results. Generally, deposition in high aspect ratio structures by physical deposition technique such as evaporation and sputtering is limited to 0.2 step coverage.[18] Ag deposition has also been demonstrated by metal organic chemical vapor deposition with a 0.8 step coverage on patterned SiO_2 substrate with a 7:1 aspect ratio for about 70 nm Ag film[19] and by atomic layer deposition technique on patterned Si substrate with an 8:1 aspect ratio for about 40 nm Ag film.[9] The results here show the possibility to also use an adhesion and barrier layer in the trenches such as Ti/TiN (Fig. 9), Co, or Ni during Ag plasma assisted atomic layer deposition, which is necessary for real interconnects application in microelectronics. The metallic surfaces such as Co, Ni, and Ti can act as adhesion layers for plasma assisted atomic layer deposition of the silver films. The growth of the silver layer seems to be rough on tungsten (W) with the native oxide, and this may not be a good choice of adhesion layer for silver deposition by PALD.

C. Ag PALD film investigation with spectroscopic ellipsometry

The changes in the optical properties of Ag PALD layers grown on SiO_2 (26 nm)/Si substrate were studied with spectroscopic ellipsometry *ex situ* for varying PALD cycles. The ellipsometric measurements (Fig. 10) show a predominant increase in the angle ψ from 2.3 to 3 eV energy range, as the number of deposition cycles is increased, while Δ decreases as the deposition cycle is increased. ψ is an indication of reflectivity of the film, while Δ is the phase difference between the two orthogonal S and P reflected polarizations. The Ag film therefore becomes more reflective for thicker layers. In Ag PVD film, the ellipsometric angle ψ is constant at 45° between 1.5 and 3.5 eV for a continuous and thick silver layer.[20] For comparison, 40–50 nm silver layers were deposited with electron beam evaporation, and the ψ value for this PVD layer is almost constant at 44° for photon energy below 3.7 eV. On the other hand, for 3068 cycles (about 97 nm) Ag PALD grown film, the ψ value is not constant

RIGHTSLINK

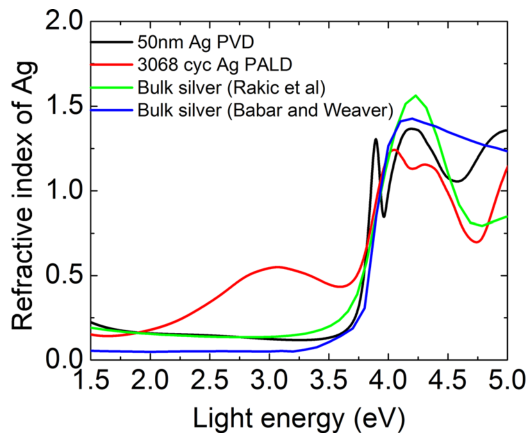

FIG. 11. (Color online) Light energy dependent refractive index of PALD and PVD Ag films compared to data from literature.

below 3.7 eV, rather it was higher below 2 eV and lower between 2 and 3.75 eV. This could be an indication that the Ag PALD may not give perfectly closed (continuous) layers even with larger number of PALD cycles.

The relative permittivity and refractive index depending on incident light energy were obtained from the ellipsometric spectrum by fitting all the optical parameters together with the film thickness for transparent layers using Brendel oscillator model in the ellipsometer database. The film thicknesses of the nontransparent layers (1500 and 3068 cycles) were also determined from XRF and SEM cross section, and this was taken into account during the fit.

That is, for the nontransparent layers, the thickness was kept constant to the measured value with SEM and XRF, while all the other optical parameters were fitted.

In addition, the maximum mean squared error obtained between the measured data and the fit was about 1. The mean squared error (MSE) is defined as[21]

$$\mathrm{MSE} = \frac{1}{\mathrm{N}-\mathrm{m}-1}\sum_{j=1}^{N}\left[\rho_{\exp}(\lambda_{\mathrm{j}}) - \rho_{\mathrm{calc}}(\lambda_{\mathrm{j}}, \mathrm{z})\right]^2,$$

where N is the total number of data points taken, $\rho_{\exp}(\lambda_{\mathrm{j}})$ is the experimental data point (typically ψ and Δ) taken at a particular wavelength λ_{j}, $\rho_{\mathrm{calc}}(\lambda_{\mathrm{j}}, \mathrm{z})$ is the calculated data point at λ_{j}, z is a vector of the fitted parameters, and m is the dimensionality of z.

The refractive index of PALD silver (about 97 nm for 3068 cycles) was compared with that of Ag PVD and bulk values (Fig. 11) found in the literature.[22,23] Ag PALD had different optical properties from the Ag PVD layers, because the PVD layers should generally have less film contamination and also closer film morphology. The imaginary part and real part of dielectric function (Fig. 12) obtained is also similar to the one obtained in literature.[20,24,25] Marsillac *et al.*[25] described in detail the three types of plasmon resonances found in the silver layers in the broadband range from 0.75 to 6.5 eV, which are intraband transitions (far infrared region), particle plasmon polariton (mid energy region), and interband transitions (ultraviolet region). Two features can be clearly seen in the dielectric functions obtained from the fit from 1.5 to 5 eV, which are the particle plasmon polariton (1.5 to 3 eV) and interband transition (just above 3.8 eV). From the imaginary part of the dielectric function in Fig. 12(a), one can see that the amplitude of the particle plasmon polariton (PPP) increases and also red shifted as the number of PALD cycles increases from 200 cycles until 1200 cycles, while just above 1200 cycles, the amplitude of PPP decreases—a trend which was also observed in Ref. 25. It can be concluded that the silver layers were initially unconnected islands as also observed in the AFM images, until after 1200 cycles (percolation threshold), the growth tends to move toward bulk regime (island are getting connected). In addition, the amplitude of interband transition increases as the silver grows into bulk regime. The infrared response of the real part of the dielectric function [Fig. 12(b)] also falls to below zero when the film begins conductivity,[24] which starts from 1500 cycles, but the measured resistivity was still quite high (above 9.4 Ω cm) after 1500 cycles (about 47 nm Ag). After 3068 PALD cycles, the film resistivity decreased sharply. A resistivity of 5.7×10^{-6} Ω cm was obtained for approximately 97 nm thick Ag film.

The morphology of conducting PALD Ag films are shown in Fig. 13. The thicker Ag layer [Fig. 13(b)] had larger grains which will mitigate electron surface scattering and grain boundary scattering effects leading to improved conductivity. Therefore, interconnected and large island size film without film impurities improves the film conductivity.

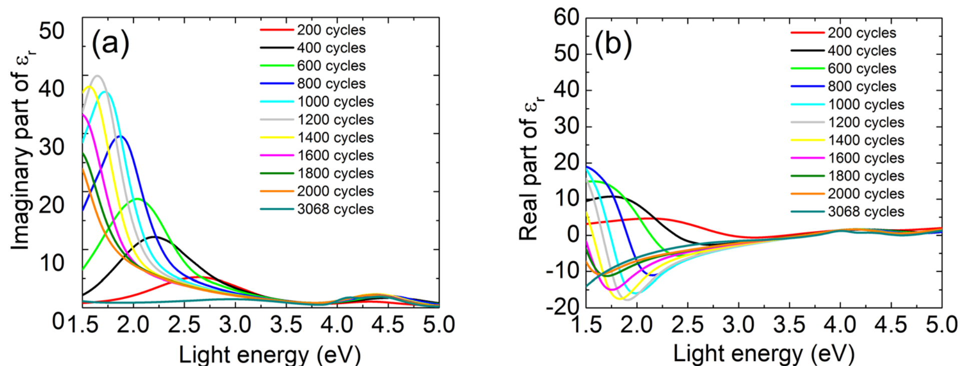

FIG. 12. (Color online) Relative permittivity of Ag films depending on light energy after different number of PALD cycles: (a) imaginary part of the relative permittivity and (b) real part of the relative permittivity.

RIGHTSLINK

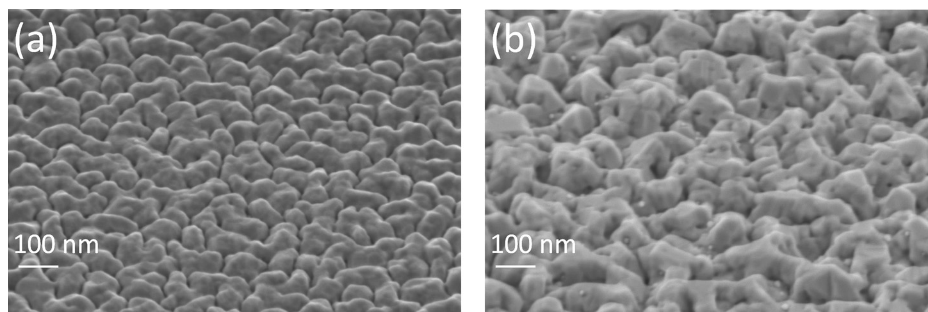

FIG. 13. SEM images of conducting PALD Ag film on silicon oxide: (a) 1500 PALD cycles (approx. 47 nm film thickness), (b) 3068 PALD cycles (approx. 97 nm film thickness).

IV. SUMMARY AND CONCLUSIONS

Silver layers have been experimentally demonstrated to grow by the remote plasma assisted atomic layer deposition with good adhesion properties and without significant film impurities on different surfaces, which are silicon substrates covered with thin films of nickel, cobalt, titanium nitride, titanium/titanium nitride, and silicon oxide. For a better Ag conductivity, the deposition temperature should be high enough that the hydrogen plasma completely removes the Ag precursor ligand. The growth and coalescence of Ag by PALD can be faster on metallic substrates with higher surface energy such as cobalt and nickel. In addition to Ti/TiN, cobalt and nickel can also act as adhesion layers for the growth of the silver films by PALD. Although silver grows by PALD on tungsten substrate, its adhesion was quite poor, possibly because of the low surface energy of the native tungsten oxide. The ellipsometric measurements show that the optical properties of the PALD Ag layers were different from those of the PVD layers. The PALD Ag layers were composed of isolated particles for thin layers until percolation threshold was reached, and the film tends toward bulk regime as the thickness increased, while the PVD layers gave closer film morphology. The conductive silver layers were polycrystalline cubic silver with a resistivity of $5.7 \times 10^{-6}\ \Omega$ cm at about 97 nm film thickness (3068 PALD cycles). For future work, it would be interesting to investigate whether *in situ* deposition of the high surface energy adhesion layers such as cobalt, nickel, and tungsten together with silver by PALD can help to grow uniform thin silver layers. In addition, further investigation needs to be carried out to check if growth of smooth silver layers on tungsten by PALD is promoted after the complete removal of native tungsten oxide.

ACKNOWLEDGMENTS

The financial support from the Investment Bank Berlin and EFRE within the framework of the Epilogos project is gratefully acknowledged. J. Bläsing and B. Garke of the Institute for Experimental Physics, Otto von Guericke University Magdeburg, are both acknowledged for taking XRD and XPS measurements, respectively.

[1] International Technology Roadmap for Semiconductors, Interconnects (2013).
[2] R. Manepalli, F. Stepniak, S. A. Bidstrup-Allen, and P. A. Kohl, IEEE Trans. Adv. Pack. **22**, 4 (1999).
[3] E. Cleveland, O. J. Glembocki, and S. M. Prokes, Proc. SPIE **8467**, 84670H (2012).
[4] M. Boccas, T. Vucina, C. Araya, E. Vera, and C. Ahhee, Thin Solid Films **502**, 275 (2006).
[5] A. P. Piedade, M. T. Vieira, A. Martins, and F. Silva, Nanotechnology **18**, 105103 (2007).
[6] M. A. Butler and A. J. Ricco, Appl. Phys. Lett. **53**, 1471 (1988).
[7] A. J. Nagy, G. Mestl, and R. Schlögl, J. Catal. **188**, 58 (1999).
[8] M. Kariniemi, J. Niinistö, T. Hatanpää, M. Kemell, T. Sajavaara, M. Ritala, and M. Leskelä, Chem. Mater. **23**, 2901 (2011).
[9] A. Niskanen, T. Hatanpää, K. Arstila, M. Leskelä, and M. Ritala, Chem. Vap. Deposition **13**, 408 (2007).
[10] F. J. van den Bruele, M. Smets, A. Illiberi, Y. Creyghton, P. Buskens, F. Roozeboom, and P. Poodt, J. Vac. Sci. Technol., A **33**, 01A131 (2015).
[11] H. E. Porteanu, R. Gesche, and K. Wandel, Plasma Sources Sci. Technol. **22**, 035016 (2013).
[12] D. Bonn, J. Eggers, J. Indekeu, J. Meunier, and E. Rolley, Rev. Mod. Phys. **81**, 739 (2009).
[13] C. T. Campbell, Surf. Sci. Rep. **27**, 1 (1997).
[14] J. W. Clancey, A. S. Cavanagh, R. S. Kukreja, A. Kongkanand, and S. M. George, J. Vac. Sci. Technol., A **33**, 01A130 (2015).
[15] L. Baker, A. S. Cavanag, J. Yin, S. M. George, A. Kongkanand, and F. T. Wagner, Appl. Phys. Lett. **101**, 111601 (2012).
[16] L. Vitos, A. V. Ruban, H. L. Skriver, and J. Kollar, Surf. Sci. **411**, 186 (1998).
[17] I. N. Yakovkin and M. Gutowski, Surf. Sci. **601**, 1481 (2007).
[18] H. Kim, J. Vac. Sci. Technol., B **21**, 2231 (2003).
[19] E. T. Eisenbraun, A. Klaver, Z. Patel, G. Nuesca, and A. E. Kaloyeros, J. Vac. Sci. Technol., B **19**, 585 (2001).
[20] T. W. H. Oates, H. Wormeester, and H. Arwin, Prog. Surf. Sci. **86**, 328 (2011).
[21] H. Tompkins and E. A. Irene, *Handbook of Ellipsometry* (William Andrew, New York, 2005).
[22] S. Babar and J. H. Weaver, Appl. Opt. **54**, 477 (2015).
[23] A. D. Rakić, A. B. Djurišić, J. M. Elazar, and M. L. Majewski, Appl. Opt. **37**, 5271 (1998).
[24] T. W. H. Oates and A. Mücklich, Nanotechnology **16**, 2606 (2005).
[25] S. Marsillac, S. A. Little, and R. W. Collins, Thin Solid Films **519**, 2936 (2011).

RIGHTSLINK